Article:

eprints@whiterose.ac.uk
https://eprints.whiterose.ac.uk/

Design and characterization of high optical quality InGaAs/GaAs/AlGaAs-based polariton microcavities

L. Tinkler, P. M. Walker, E. Clarke, D. N. Krizhanovskii, F. Bastiman, M. Durska, and M. S. Skolnick

Articles you may be interested in

Design and characterization of high optical quality InGaAs/GaAs/AlGaAs-based polariton microcavities

L. Tinkler,[1,a)] P. M. Walker,[1] E. Clarke,[2] D. N. Krizhanovskii,[1] F. Bastiman,[2] M. Durska,[1] and M. S. Skolnick[1]

[1]*Department of Physics and Astronomy, University of Sheffield, Sheffield S3 7RH, United Kingdom*
[2]*EPSRC National Centre for III-V Technologies, University of Sheffield, Sheffield S1 3JD, United Kingdom*

The presence of dislocations arising from strain relaxation strongly affects polaritons through their photonic component and ultimately limits experiments involving polariton propagation. In this work, we investigate the range of growth parameters to achieve high optical quality GaAs/Al_xGa_{1-x}As-based microcavities containing strained In_xGa_{1-x}As quantum wells and using differential interference contrast (Nomarski) microscopy deduce a design rule for homogeneous versus disordered structures. We illustrate the effect of disorder by contrasting observations of polariton condensates in relaxed and unrelaxed microcavities. In our optimized device, we generate a polariton condensate and deduce a lifetime for the interacting polariton fluid of 39 ± 2 ps. © 2015 AIP Publishing LLC. [http://dx.doi.org/10.1063/1.4905907]

Microcavity polaritons are the quasi-particles arising from the strong-coupling between quantum well (QW) excitons and photons. Since their first observation polaritons have attracted a great deal of attention as they open the solid-state up to investigations into a wide range of phenomena such as condensation,[1] superfluidity,[2] vortices, and solitons.[3,4] Furthermore, polaritons promise applications in devices such as amplifiers,[5] transistors,[6] and logic elements.[7] However, for all of these, we require microcavities with little, or no in-plane disorder.

A typical microcavity structure consists of two distributed Bragg-reflector (DBR) mirrors forming a Fabry-Pérot cavity containing several QWs. The DBR mirrors are formed by alternate layers of materials with contrasting refractive indices. The reflectivity of these mirrors and the subsequent Q-factor of the cavity are determined by the index contrast between the layers and the number of repeats. Despite the similarity in lattice constants (0.14% at room temperature) of GaAs and AlAs, the large number of layers required to achieve high reflectivity mean significant strain may be accumulated in the structure. This strain may be relieved via dislocations which form a characteristic crosshatch pattern.[8] Disorder in microcavities strongly modulates the potential experienced by polaritons through the photonic component and may result in partial[9] or even total polariton confinement.[10]

Similarly, the Rabi splitting exhibited by a microcavity is dependent upon the number and the confinement energy (depth) and hence exciton oscillator strength of the QWs. Using In_xGa_{1-x}As QWs has the advantage that the GaAs substrate is transparent for the emission wavelength allowing for experiments in the transmission configuration. However, the mismatch in lattice constants means that increasing either the depth or number of QWs serves to increase the strain in the structure. Therefore, the design of microcavity devices is a compromise between figures of merit—such as the Q-factor and Rabi splitting—and the accumulation of strain

which may lead to in-plane disorder. Several schemes have been proposed to compensate for this lattice mismatch, through the use of pseudo-alloys[11] or by incorporation of strain compensating layers of AlP in the DBR layers.[12] However, the growth of high-quality and homogeneous microcavities remains a technical obstacle to fundamental research and to the development of polaritonic devices.

The energy stored per unit area in a bilaterally strained elastically isotropic material is[13]

$$E_{st} = 2G\frac{1+\sigma}{1-\sigma}\epsilon_\parallel^2 h, \tag{1}$$

where h is the layer thickness, G is the shear modulus of the material, σ is Poisson's ratio, and $\epsilon_\parallel$ is the in-plane strain arising from the mismatch in lattice constants between the film (a_f) and substrate (a_s)

$$\epsilon_\parallel = \frac{a_s - a_f}{a_f}. \tag{2}$$

For a microcavity, Eq. (1) becomes the sum over all layers. Additionally, in the absence of strain relaxation, the lattice constant perpendicular to the growth direction is fixed throughout the structure by the substrate. Therefore, given the material constants[14] for each layer, the strain energy density for a particular microcavity design can be calculated.

In the People and Bean[13] model, the strain energy density is equated with that associated with a dislocation to yield a critical layer thickness (h_c) above which defects form spontaneously to partially relieve the strain. Using Eq. (9a) from Ref. 13 and the material parameters[24,25] for AlAs on GaAs at 590 °C, this was calculated to give $h_c \sim 50\,\mu$m. In the Matthews and Blakeslee model,[8] the mechanical forces along a threading dislocation are equated to give a much lower critical thickness above which existing defects are propagated through a multilayer structure. Using Eq. (5) from Ref. 8 for AlAs on GaAs at 590 °C, $h_c \sim 1\,\mu$m. Without knowing the origin of the crosshatch disorder, it is difficult

a)Electronic mail: l.tinkler@sheffield.ac.uk

TABLE I. Microcavity designs detailing aluminum content and number of repeats in the upper (U) and lower (L) DBR mirrors and the indium content, and number of QWs.

Sample	Al (%)	U(L) DBR	In (%)	QWs
1	100	25(27)	6	6
2	100	21(22)	4	1
3	85	23(26)	4	1
4	85	23(26)	4	3
5	85	23(26)	6	6

to predict what design of microcavity would lead to strain relaxation. Therefore, in this work, we systematically investigate the range of design parameters for the growth of microcavities without in-plane disorder, using differential interference contrast (Nomarski) microscopy to identify a limit on the strain energy density before the onset of strain relaxation. We illustrate the effect of such in-plane disorder by comparing observations of polariton condensates in relaxed- and unrelaxed-samples.

All our designs consist of DBRs formed of alternate layers of GaAs and $Al_xGa_{1-x}As$ and an $n/2\lambda$ GaAs cavity containing one or more $In_xGa_{1-x}As$ QWs. The thickness of the QW layers was 10 nm in all except sample 3 which contained one 8 nm well. Table I details the composition and number of DBR layers and QWs in each design. The samples were grown by molecular beam epitaxy on GaAs(100) substrates with all layers grown at a standard growth temperature of 590 °C to obtain high quality GaAs and AlGaAs, except for the InGaAs QWs and subsequent 10 nm of GaAs which were grown at 500 °C.

Fig. 1 shows Nomarski micrographs of samples 1 and 2. Both show a crosshatch pattern arising from stress relaxation along the [110] and [1$\bar{1}$0] directions. The high density of crosshatching in sample 1 is indicative of the strain energy accumulated in the large number of DBR layers and QWs. It was shown by Zajac, Langbein, and Clarke that even an empty cavity with a similar number of DBR repeats may undergo strain relaxation.[12] In sample 2, the number of DBR repeats and QWs, and thus total strain is reduced, which is reflected in the reduced level of crosshatching.

Samples 1 and 2 also contain a number of "oval" defects attributed to droplets emitted by the gallium cell during growth.[15] Whist these do not contribute to crosshatch disorder, they do affect the potential landscape. These defects were eliminated in later samples by increasing the cell tip temperature and out-gassing.
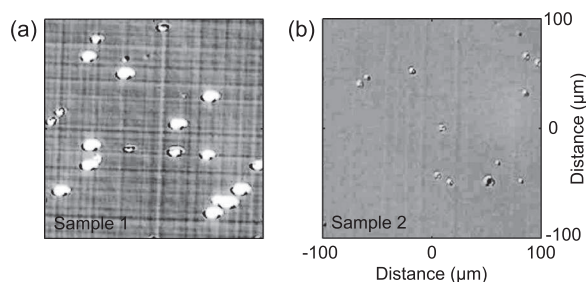
FIG. 1. Nomarski micrographs of microcavity samples with AlAs/GaAs DBR mirrors and containing six $In_{0.06}Ga_{0.94}As$ QWs (a) and one $In_{0.04}Ga_{0.96}As$ QW (b). Identical scale used in each panel.
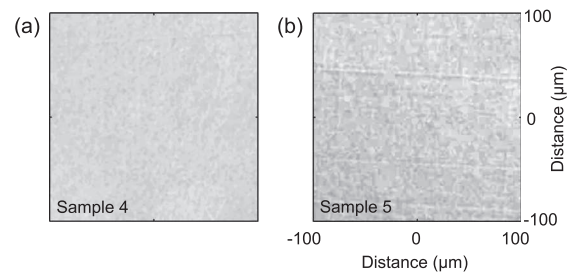
FIG. 2. Nomarski micrographs of microcavity samples with $Al_{0.85}Ga_{0.15}As/$GaAs DBR mirrors containing three $In_{0.04}Ga_{0.96}As$ QWs (a) and six $In_{0.06}Ga_{0.94}As$ QWs (b). Identical scale used in each panel.

Using $Al_{0.85}Ga_{0.15}As$ in the DBR reduces the lattice mismatch with GaAs and thus the strain accumulated. However, this reduces the index contrast in the mirror pairs and so more repeats are required to maintain a similar Q-factor. Fig. 2 shows Nomarski micrographs of microcavity samples containing 23(26) repeats of $Al_{0.85}Ga_{0.15}As/$GaAs in the upper (lower) DBR mirrors. Fig. 2(a) shows a Nomarski micrograph of sample 4 which contains three $In_{0.04}Ga_{0.96}As$ QWs and shows no visible sign of disorder. Sample 3, which contains just one $In_{0.04}Ga_{0.96}As$ QW, was similarly unrelaxed.

Finally, increasing the number or the strength of the QWs enhances the coupling between the photon and exciton modes but also contributes to the total strain. From the Nomarski micrograph of sample 5 shown in Fig. 2(b), the additional strain from six $In_{0.06}Ga_{0.94}As$ QWs is sufficient to cause strain relaxation.

Using Eq. (1), the strain energy which would be stored in a particular design of microcavity in the absence of strain relaxation was calculated. Fig. 3 shows results of this calculation for each design at various temperatures, which shows a clear division between the relaxed and unrelaxed samples: with the relaxed samples 1, 2, and 5 all lying to the upper part of the figure and the unrelaxed samples 3 and 4 lying in the lower part. At the growth temperature (590 °C), this division occurs at a strain energy density of 0.35 ± 0.01 J m^{-2}, placing a limit on the strain energy density before the onset of strain relaxation. This was confirmed by repeated growths of samples 2, 3, and 4.

On comparing this to the energy stored in a critically thick layer of AlAs on GaAs at 590 °C using the expressions from Refs. 13 and 8, we find that all the lines in Fig. 3 lie between the critical values predicted by the two theories.
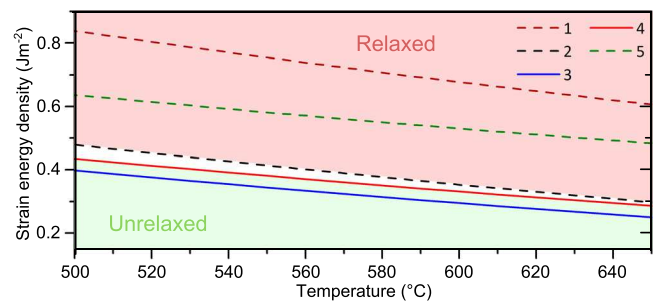
FIG. 3. Calculated strain energy density versus temperature for microcavity designs 1–5. Samples which showed evidence of crosshatch disorder are indicated by dashed lines. Shaded areas indicate regions where all samples were relaxed or unrelaxed, respectively.

That is, the strain energy density calculated for all designs is above that required to propagate threading dislocations from grown-in defects (0.11 J m^{-2}) but well below that to spontaneously form new defects (5.3 J m^{-2}). The system is thus well away from mechanical equilibrium at which we would expect to observe crosshatching above the Matthews and Blakeslee limit. The limit we identify in this study therefore corresponds to the edge of a metastable region where grown-in defects are insufficiently mobile to result in observable strain relaxation within the growth time (see Ref. 16).

To illustrate the effect of disorder upon polariton phenomena, we compare the optical properties of relaxed and unrelaxed microcavity samples. Samples 1 and 4 were placed in a continuous-flow helium vapor cryostat and held at approximately 5 K. Excitation was provided by a tunable Ti:sapphire laser focused to a 30 μm spot incident at 15° ($k_x \approx 1.9 \mu$m^{-1}). The photoluminescence (PL) emission or its Fourier transform was then imaged onto the entrance slit of a single-grating spectrometer equipped with a CCD camera.

From angle-resolved PL measurements using non-resonant excitation, sample 4 exhibits a vacuum Rabi splitting of 4.4 meV and a resolution limited lower polariton linewidth of 0.10 meV, corresponding to a Q-factor in excess of 15 000. The cavity-exciton detuning varies across the sample due to a rotation stop during growth. Fig. 4(a) shows the observed PL spectrum, the fitted polariton dispersion, and deduced uncoupled exciton- and cavity-modes. The detuning was chosen to be slightly negative (−2.1 meV).

The laser was brought into resonance with the lower polariton branch by tuning the energy and incidence angle. In this optical parametric oscillator (OPO)[17] configuration, pairs of pump polaritons are scattered to the ground state and to an idler state at twice the pump wavenumber. Above a threshold power density, this parametric scattering process becomes stimulated leading to macroscopic occupation of the ground state. For sample 4, this occurs at a threshold power density of $P_{th} = 1.5$ kW cm^{-2} and is accompanied by a nonlinear increase in emission intensity from the ground state, and narrowing in momentum space. This is shown in Fig. 4(b) in the angle-resolved spectrum of the emission taken from a 30 μm diameter spot at the center of the condensate at $P = 5P_{th}$. Fig. 4(c) shows the corresponding real-space image of the PL emission in which the condensate has a smoothly varying spatial distribution (see line-cut in Fig. 4(d)), consistent with the results of Nomarski microscopy.

Above threshold, the predominantly repulsive polariton-polariton interactions within the condensate result in a local renormalization of the dispersion by 0.28 meV. As a consequence polaritons are expelled from the condensate with a well defined momentum, their excess energy being transformed into kinetic energy.[18] This results in an isoenergetic ring in momentum space shown in Fig. 4(e), the radius of which is determined by the renormalization energy of the condensate and the wavenumber corresponding to this energy in the low density region. This is illustrated in Fig. 4(f), which shows angle-resolved PL measurements taken from 30 μm regions at the center and 80 μm away from the condensate.

The intensity of the expelled polaritons decays exponentially away from the condensate on a characteristic length of $l = 45.8 \pm 0.5 \mu$m (Fig. 4(d)). The group velocity of these
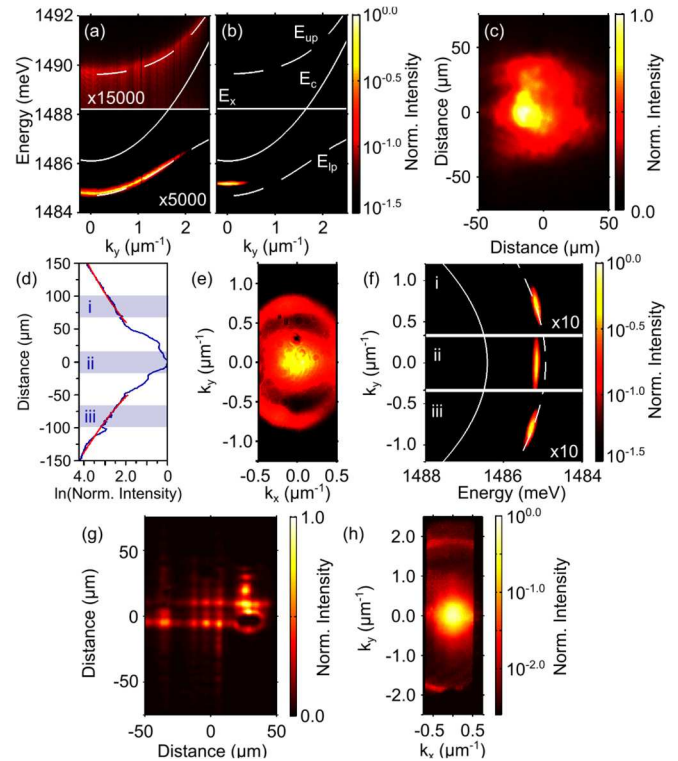
FIG. 4. Angle-resolved photoluminescence spectrum of emission from sample 4 with non-resonant excitation (a) and above threshold (b) showing fitted polariton dispersion (dashed) and deduced exciton- and cavity-modes (solid). Pseudo-color real-space image of condensate (c) and natural logarithm of emission intensity along a vertical cut at $x = -15 \mu$m (d) showing fitted exponential decay away from condensate (red). Distribution of emission in momentum space above threshold (e). Angle-resolved photoluminescence spectra taken 80 μm above (i), below (iii), and at the center (ii) of the condensate (f). Pseudo-color real space image of condensate in sample 1 (g) and distribution in momentum space (h). Panels (a) and (b), and (e) and (f) share a color scale.

polaritons is defined by the dispersion of the lower polariton branch.[19] For the expelled polaritons at $k_y = 0.74 \pm 0.02 \mu$m^{-1}, $v_g = 1.18 \pm 0.06 \mu$m ps^{-1}. We therefore obtain a lifetime for the polariton fluid of 39 ± 2 ps from $\tau_{pol} = l/v_g$[20] which, due to interaction with the pump, may differ from the free particle lifetime. This is comparable to reports of tens of picoseconds in similar optimized systems[4,21] and up to 100 s of picoseconds in ultra-high-Q microcavities.[22]

Fig. 4(g) shows a pseudo-color image of the emission in the strongly relaxed sample under similar conditions in which the condensate is strongly fragmented, forming in a regular lattice pattern in sympathy with the crosshatch disorder.[23] The emission from the bright spots increases nonlinearly above threshold and is accompanied by a narrowing in linewidth and renormalization of the dispersion. Fig. 4(h) shows the narrow distribution of emission in momentum space above threshold as well as the presence of a clear ring at $|k_{\parallel}| \approx 1.9 \mu$m^{-1} corresponding to the Rayleigh scattering of pump polaritons,[26] indicating the presence of a large number of scattering centers. This Rayleigh ring was not observed in the unrelaxed sample.

In conclusion, the presence of crosshatch disorder arising from strain relaxation strongly affects the spatial uniformity of polariton condensates by modulating the potential landscape, ultimately limiting possible experiments involving polariton

propagation. Using Nomarski microscopy, we identify a limit on the strain energy density for disorder-free $Al_xGa_{1-x}As$/GaAs-based microcavities containing $In_xGa_{1-x}As$ QWs. This limit can be used as a design rule for future microcavity devices for use in transmission-based experiments into solitons, vortices, or superfluidity.

We note that since our submission Cilibrizzi and co-workers have reported the growth of a GaAs-based microcavity containing InGaAs QWs using AlAsP/GaAs in the DBR layers to prevent strain build-up.[27]

[1]J. Kasprzak, M. Richard, S. Kundermann, A. Baas, P. Jeambrun, J. M. J. Keeling, F. M. Marchetti, M. H. Szymańska, R. André, J. L. Staehli, V. Savona, P. B. Littlewood, B. Deveaud, and L. Si Dang, Nature **443**, 409 (2006).

[2]A. Amo, D. Sanvitto, F. P. Laussy, D. Ballarini, E. del Valle, M. D. Martin, A. Lemaître, J. Bloch, D. N. Krizhanovskii, M. S. Skolnick, C. Tejedor, and L. Viña, Nature **457**, 291 (2009).

[3]M. Sich, D. N. Krizhanovskii, M. S. Skolnick, A. V. Gorbach, R. Hartley, D. V. Skryabin, E. A. Cerda-Méndez, K. Biermann, R. Hey, and P. V. Santos, Nat. Photonics **6**, 50 (2011).

[4]A. Amo, S. Pigeon, D. Sanvitto, V. G. Sala, R. Hivet, I. Carusotto, F. Pisanello, G. Leménager, R. Houdré, E. Giacobino, C. Ciuti, and A. Bramati, Science **332**, 1167 (2011).

[5]E. Wertz, A. Amo, D. D. Solnyshkov, L. Ferrier, T. C. H. Liew, D. Sanvitto, P. Senellart, I. Sagnes, A. Lemaître, A. V. Kavokin, G. Malpuech, and J. Bloch, Phys. Rev. Lett. **109**, 216404 (2012).

[6]T. Gao, P. S. Eldridge, T. C. H. Liew, S. I. Tsintzos, G. Stavrinidis, G. Deligeorgis, Z. Hatzopoulos, and P. G. Savvidis, Phys. Rev. B **85**, 235102 (2012).

[7]T. C. H. Liew, A. V. Kavokin, and I. A. Shelykh, Phys. Rev. Lett. **101**, 016402 (2008).

[8]J. W. Matthews and A. E. Blakeslee, J. Cryst. Growth **27**, 118 (1974).

[9]F. Manni, K. G. Lagoudakis, B. Pietka, L. Fontanesi, M. Wouters, V. Savona, R. André, and B. Deveaud-Plédran, Phys. Rev. Lett. **106**, 176401 (2011).

[10]J. M. Zajac, W. Langbein, M. Hugues, and M. Hopkinson, Phys. Rev. B **85**, 165309 (2012).

[11]U. Oesterle, R. P. Stanley, and R. Houdré, Phys. Status Solidi B **242**, 2157 (2005).

[12]J. M. Zajac, E. Clarke, and W. Langbein, Appl. Phys. Lett. **101**, 041114 (2012).

[13]R. People and J. C. Bean, Appl. Phys. Lett. **47**, 322 (1985).

[14]The material parameters for GaAs, AlAs, and InAs are taken from Ref. 24 from which the properties of their ternary alloys were calculated assuming a linear relationship. The thermal expansion coefficient of GaAs was taken from Ref. 25.

[15]H. Kawada, S. Shirayone, and K. Takahashi, J. Cryst. Growth **128**, 550 (1993).

[16]J. Y. Tsao, B. W. Dodson, S. T. Picraux, and D. M. Cornelison, Phys. Rev. Lett. **59**, 2455 (1987).

[17]R. M. Stevenson, V. N. Astratov, M. S. Skolnick, D. M. Whittaker, M. Emam-Ismail, A. I. Tartakovskii, P. G. Savvidis, J. J. Baumberg, and J. S. Roberts, Phys. Rev. Lett. **85**, 3680 (2000).

[18]E. Wertz, L. Ferrier, D. D. Solnyshkov, R. Johne, D. Sanvitto, A. Lemaître, I. Sagnes, R. Grousson, A. V. Kavokin, P. Senellart, G. Malpuech, and J. Bloch, Nat. Phys. **6**, 860 (2010).

[19]The group velocity (v_g) is defined by the derivative of energy with respect to in-plane wavenumber ($k_{\parallel}$). For the lower polariton branch,

$$E_{lp}(k_{\parallel}) = \frac{1}{2}\left(E_c(k_{\parallel}) + E_x - \sqrt{\Omega^2 + \Delta^2}\right),$$

where Ω is the Rabi splitting, E_x is the exciton transition energy, $E_c(k_{\parallel})$ is the cavity photon energy, and $\Delta = E_c(k_{\parallel}) - E_x$.

Around $k_{\parallel} = 0$, the dispersion of cavity photons is parabolic. We may therefore write

$$E_c(k_{\parallel}) = E_c(k_{\parallel} = 0) + \frac{\hbar^2 k_{\parallel}^2}{2m^*},$$

where m^* is the effective mass of cavity photons. From the fitted dispersion, we find $m^* = 4.45 \pm 0.03 \times 10^{-35}$ kg. Taking the derivative of first equation mentioned in this reference with respect to $k_{\parallel}$, the group velocity of polaritons in the lower polariton branch is

$$v_g = \frac{1}{2}\left(1 - \frac{\Delta}{\sqrt{\Omega^2 + \Delta^2}}\right)\frac{\hbar k_{\parallel}}{m^*}.$$

[20]The deduced polariton lifetime was corroborated by a direct measurement of the decay in emission intensity using a streak camera in subsequently fabricated microcavity wires. (J. K. Chana and M. Sich (unpublished)).

[21]R. Hivet, H. Flayac, D. D. Solnyshkov, D. Tanese, T. Boulier, D. Andreoli, E. Giacobino, J. Bloch, A. Bramati, G. Malpuech, and A. Amo, Nat. Phys. **8**, 724 (2012).

[22]B. Nelsen, G. Liu, M. Steger, D. W. Snoke, R. Balili, K. West, and L. Pfeiffer, Phys. Rev. X **3**, 041015 (2013).

[23]D. Sanvitto, D. N. Krizhanovskii, D. M. Whittaker, S. Ceccarelli, M. S. Skolnick, and J. S. Roberts, Phys. Rev. B **73**, 241308(R) (2006).

[24]O. Madelung, *Semiconductors: Data Handbook*, 3rd ed. (Springer-Verlag, 2004).

[25]S. Adachi, J. Appl. Phys. **58**, R1 (1985).

[26]W. Langbein and J. M. Hvam, Phys. Rev. Lett. **88**, 047401 (2002).

[27]P. Cilibrizzi, A. Askitopoulos, M. Silva, F. Bastiman, E. Clarke, J. M. Zajac, W. Langbein, and P. G. Lagoudakis, Appl. Phys. Lett. **105**, 191118 (2014).